Exact Coherent Structures with Broken Symmetry in Plane Couette Flow

---

A Thesis
Presented to
The Division of Mathematics and Natural Sciences
Reed College

In Partial Fulfillment
of the Requirements for the Degree
Bachelor of Arts

Varchas Gopalaswamy

April 5, 2015

Approved for the Division
(Physics)

Daniel Borrero

Table of Contents

List of Figures

Introduction

> I am an old man now, and when I die and go to heaven, there are two matters on which I hope for enlightenment. One is quantum electrodynamics, and the other is the turbulent motion of fluids. And about the former, I am optimistic
>
> Horace Lamb, 1932

Although much work has been done in understanding turbulence since Lamb's time, the turbulence problem remains unsolved to this day. Flow states are said to be **turbulent** if they display large spatiotemporal variations in fluid velocity, as in Figure 1. The problem itself can be stated simply – Is there a way us to begin with an initial flow state and a geometry (say, the body of an airplane), and properly predict the behavior, properties and structure of the flow state forward in time, down to the smallest scales? In this case it is deceptively simple, for much like a small, unnamed village in coastal Armorica holding out against the Romans, the turbulence problem that has confounded physicists and engineers for centuries. Understanding turbulence is vitally important, since turbulent flows appear in artificial scenarios such as the flow around ships or aircraft, and in natural scenarios from the atmosphere of Jupiter to the blood flow in the heart. Turbulent flows are typically characterized by the **Reynolds number**, which is the (dimensionless) ratio between the inertial and viscous damping forces. At small Re, viscosity dominates, and smooths out large velocity gradients in the fluid, resulting in the well-ordered **laminar** flow. At large Re, kinetic energy is dissipated at a lower rate, allowing for the existence of increasingly complex flow structures, such as eddies or vortices, which are characteristic of turbulence.

Transitions to and from Turbulence

Understanding the transition to and from turbulence states are important for both theoretical and practical reasons. Laminar flows tend to cause less drag in aerodynamic scenarios, but fluid lamina do not mix fluids efficiently, and thus are much less effective in scenarios that require efficient mixing. Turbulent flows on the other hand tend to cause more drag in aerodynamic flows, tend to mix fluids extremely quickly. In general, there are two routes by which flows transition to turbulence. In

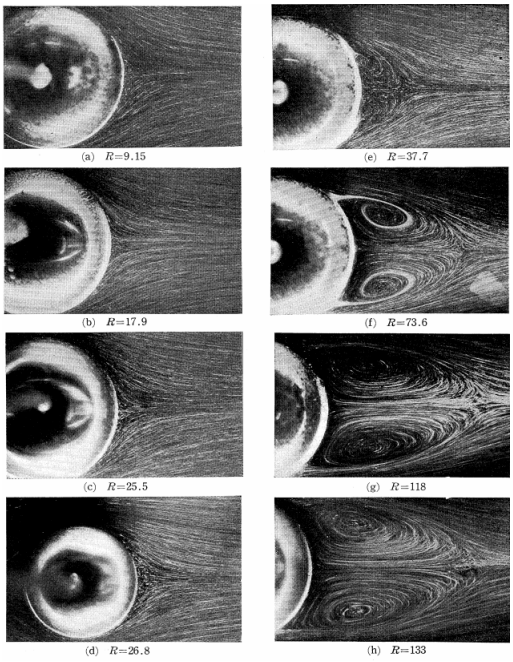

Figure 1: Representations of cylinder wakes at various Re. Notice that the flow goes from laminar in (a) to turbulent in (h), with two prominent vorticies, where velocity gradients are much higher than they were along the laminar streamlines of (a). Reproduced from S. Taneda, *Experimental investigation of the wake behind a sphere at low Reynolds numbers*, Journal of the Physical Society of Japan, 11(10):1104-1108 [1].

the supercritical transition, an increase in Re above some critical value results in the loss of stability of the laminar state[1] and the emergence of new stable solutions of higher complexity. These states eventually bifurcate into even more complex states at higher critical values, eventually resulting in turbulence. Supercritical transitions occur in Taylor-Couette flow with low outer-cylinder rotation rates, and well as in Rayleigh-Bernard convection, and are well predicted by linear stability analysis.

The second, more complex type of transition is the subcritical transition. In the subcritical transition, the laminar state loses stability at lower Re than linear stability analysis would predict, and the flow transitions *directly* to turbulence, instead of increasingly gradually in complexity. Furthermore, the laminar state remains locally stable - that is, some finite perturbation is needed to 'kick' the flow into turbulence. Subcritical transitions cannot be predicted by linear stability analysis and are, therefore, less well understood. Nevertheless can be physically important. Subcritical transitions occur in pressure-driven flows in pipes, which models flows such as those in hypodermic needles or lung alveoli, or shear-driven flow between two infinite parallel plates (displayed in Figure 2), which is known as plane Couette flow, and is the focus of this thesis [2, 3]. Systems that transition subcritically also exhibit transient turbulence, where the moderate Re turbulent flows can suddenly relaminarize, often

[1]That is to say, it is no longer stable against infinitesimal perturbations

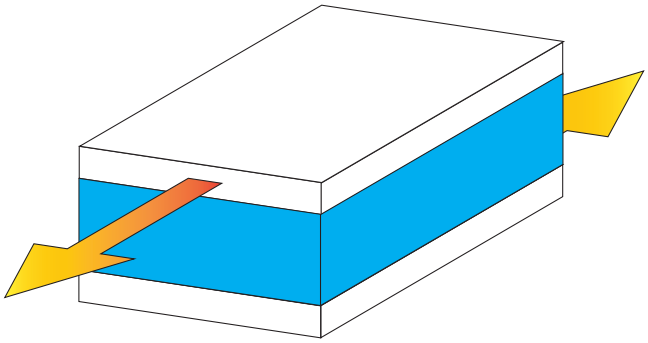

Figure 2: A diagram of the plane Couette geometry. The upper and lower plates extend infinitely in the plane, as does the fluid filling the gap. The upper and lower plates move with some constant velocity, and apply shear stresses on the fluid, resulting in fluid motion. While in general the plates can move in any direction, there is always a reference frame in which the plates move with equal but opposite velocity, and it is convenient to work in this reference frame. According to convention, the x axis is aligned along the plate velocity, and is also referred to as the **streamwise** direction, the y-axis is aligned perpendicular to the plates and is referred to as the **wall-normal** direction, and the z-axis is normal to both axes and is referred to as the **spanwise** direction.

with no obvious indication [4]. There are also a vast array of studies showing that the probability that a flow remains turbulent decays exponentially, that is

$$P(\text{Turbulent}) \propto e^{-\frac{t}{\tau}}, \tag{1}$$

in both pipe and plane Couette flows [5, 6], where τ is the 'half life' of turbulence. It is evident that τ has some Re dependence, but the functional form is not well known, nor is it known if there is some critical Re after which τ diverges and turbulence is sustained.

Plane Couette Flow

The geometry of the plane Couette system is extremely simple, with only one geometrical parameter h, the half-distance between the parallel plates, and one kinematic parameter V, the velocity of the upper plate[2], giving the Reynolds number as

$$Re = \frac{hV}{\nu}, \tag{2}$$

where ν is the kinematic viscosity. When Re is very small, only the laminar flow state is stable. In the case of plane Couette flow, this corresponds to the linear velocity profile shown in Figure 3. As Re increases, however, we would expect the emergence of long lived turbulence, which has been seen in experiments [7].

[2]While in principle the upper and lower plate can have different velocities, there should always be a reference frame in which the upper plate has velocity V, and the lower plate has velocity $-V$.

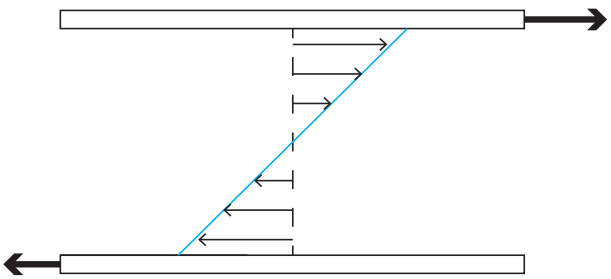

Figure 3: A cross-sectional representation of plane Couette flow, with the laminar velocity profile shown. By symmetry, the laminar profile must be the same everywhere.

Tackling Turbulence

The traditional approach towards the analysis of turbulence for the last century has been the statistical approach initially developed by Reynolds, Prandtl, von Karman, Kolmogorov and others [8]. At the core of the statistical approach to turbulence is the assumption that turbulent flow states can be expressed as random perturbations around some mean flow. At extremely high Re, where direct numerical simulation (DNS) of the flow is computationally infeasible, the statistical approach is invaluable, but at low-to-moderate Re, these models can become less accurate [8]. Even ignoring the moderate Rebehavior of the statistical models, the fundamental issue with the statistical approach is its discarding of the dynamical information about turbulence. Methods like Reynolds Averaged Navier-Stokes use a combination of time-averaging and modeling to eliminate small scale perturbations, while Large Eddy Simulations explicitly do not resolve small scale structures, and choose instead to model them. For this reason, it seems likely that while statistical methods are the foundation of computational fluid dynamics (CFD), they cannot truly provide an answer to the turbulence problem.

An alternate approach was proposed by Eberhard Hopf in 1948 [9]. Hopf suggested that solutions to the Navier-Stokes equations might be thought of as trajectories in an infinite dimensional state space in which each point corresponded to a possible velocity field. To better understand what this would mean, consider the velocity field at a point in the fluid, pictured in Figure 4. In order to describe the velocity vector, three numbers are required (each of which can take any real value), so this microsystem has three dimensions. Now any finite fluid volume will have an uncountably infinite number of points at which the velocity field has a value, so we would need an uncountably infinite set of numbers to describe any velocity field. An object that would keep track of all these numbers would form an infinite dimensional vector, so that any flow state can be represented by a particular vector in this infinite dimensional vector space, known as the **state space**. Luckily, every point in the space does not necessarily correspond to a solution of the Navier-Stokes equation; for a given finite Re, for instance, the gradient of the velocity field cannot be too large. Hopf thus conjectured that physical trajectories, corresponding to solutions to the Navier-Stokes equation would lie on some finite-dimensional manifold (known as the

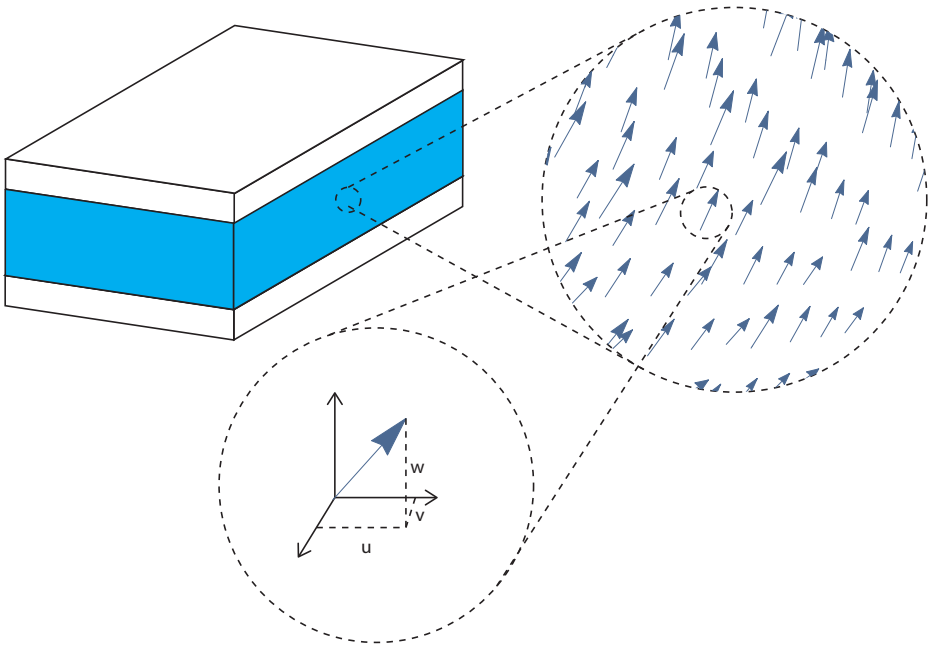

Figure 4: At each point in the fluid volume, the velocity field has a value that is described by three numbers, thus requiring three dimensions to track over time.

inertial manifold) embedded within this infinite dimensional space. The restriction of dynamics from the infinite dimensional space to a finite dimensional inertial manifold due to the variation of a control parameter has been rigorously proven under certain conditions [10]. For the Navier-Stokes equation, the inertial manifold's control parameter is Re, and physical intuition suggests that its structure should also have Re dependence, since at very low Re, the only physical solution is the laminar state, and as Re increases, more complex flows become physically permissible. Hopf proposed finally that turbulence in this view was simply a trajectory that would travel across wide distances on the manifold.

Unfortunately for Hopf, the computer power necessary to pursue this line of work was not available in 1948, leading him to comment in frustration that "the great mathematical difficulties of these important problems are well known and at present the way to a successful attack on them seems hopelessly barred". It would take until 1963 and the derivation of the Lorenz attractor (Figure 5) for the first numerical state-space analysis of turbulence [12], albeit for a highly truncated version of Navier-Stokes, designed to investigate Rayleigh-Bernard convection[3]. There have also been a number of efforts to explore the structure of invariant manifolds in moderate turbulence Navier-Stokes, such as Proper Orthogonal Decomposition [13] and the 'self-sustaining process theory' [14], but while fruitful they are nevertheless models of turbulent flow, and not an exact analysis of Navier-Stokes. Another avenue of research emerged in 1990, when Nagata computed nontrivial **equilibrium** flow states in plane

[3]Interestingly, Lorenz truncated Navier-Stoke via a Galerkin approximation, which is what `Channflow` also does, though it allows for many more Fourier modes than Lorenz did.

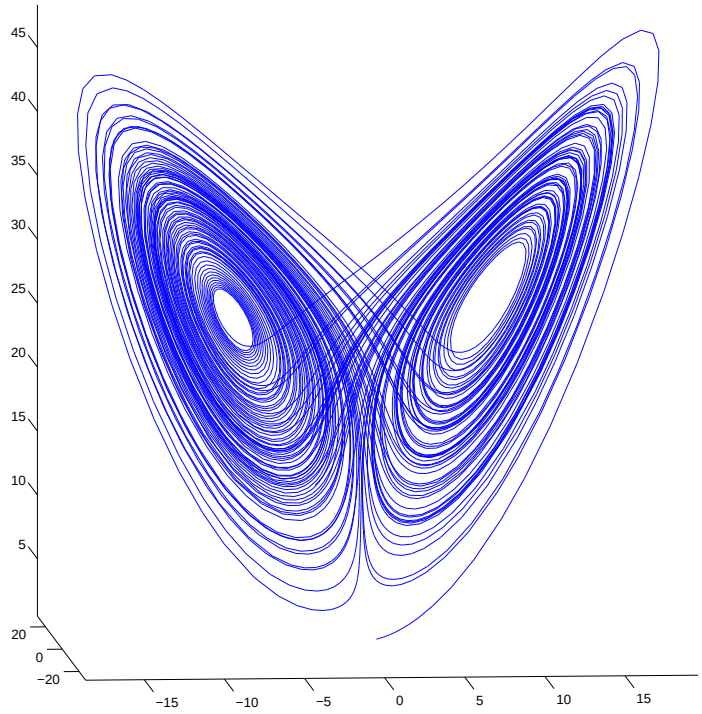

Figure 5: A plot of a particular trajectory around the Lorenz attractor. The Lorenz system is an excellent example of a system in which the dynamics exist on a sub-manifold - in this case, the space is reduced from three dimensions to the (fractal) dimension of 2.06 [11].

Couette flow by continuing the wavy vortex solution of Taylor-Couette flow [15]. This class of solutions, which were named **exact coherent structures** by Waleffe [16] are the result of calculating exact, invariant solutions of the fully resolved Navier-Stokes equation. The family of exact coherent structures was expanded with the discovery of **traveling wave equilibira** by Nagata in 1997, the computation of **periodic orbits** by Kawahara and Kida in 2001 [17], and the computation of **relative periodic orbits**[4] by Viswanath in 2007 [18]. Figure 6 summarizes the four categories of exact coherent structures. The ultimate hope of this line of research is that turbulence can be viewed as chaotic trajectories on the inertial manifold that are guided by exact coherent structures (Figure 7), implying that a fundamental understanding of exact coherent structures would lead to a better understanding of turbulent dynamics.

[4]That is, flow states that are periodic after some phase shift

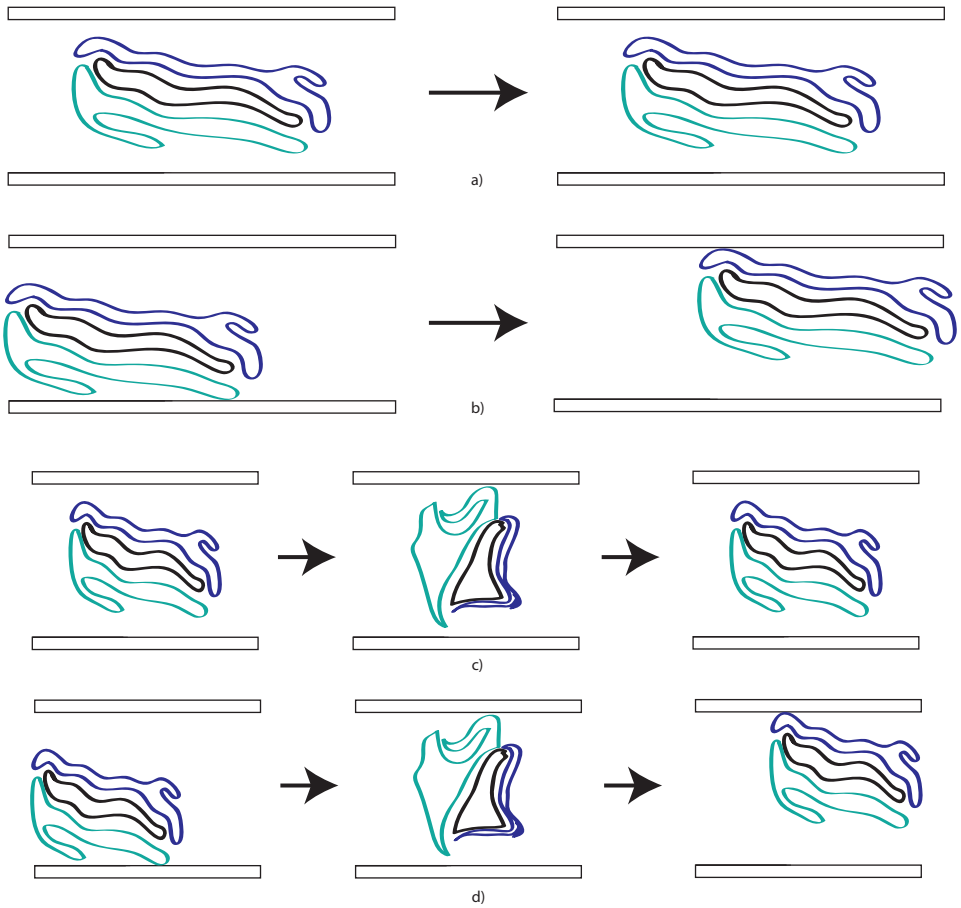

Figure 6: The four main categories of exact coherent structures. In all diagrams, only a particular velocity structure of the flow state is displayed, to demonstrate the particular type of exact coherent structures.(a) An equilibrium solution, where the fluid structure does not change over time; b), a relative equilibirum or travelling wave solution, where the state does not change in its own reference frame, but is translated relative to the observer; c), a periodic orbit, where the flow state changes over time, but returns to the original state after some period T; d), a relative periodic orbit, where the flow state is periodic in its own reference frame, but is translated relative to the observer.

While there has been a great deal of progress in this field, much of it has been computational, though experiments by Hof and de Lozar [5] are at present the only direct experimental verifications for the existence of exact coherent structures in nature. However, indirect results, such as the resemblance of the upper branch solution to the roll-streak structure seen in DNS [19], and the potential role of the stable manifold of the lower branch solution in separating the turbulent and laminar basins of attraction suggest that exact coherent structures likely play a fundamental role in the behavior and evolution of turbulent flow states. Advances in computing power, along with the development of CFD algorithms such as Channelflow [20] have also made the computation of these structures generally feasible. In order to compute the orig-

inal exact coherent structures, substantial symmetry constraints were placed upon the dynamics. This had the benefit of greatly reduced computational complexity, but has resulted in exact coherent structures that are not necessarily representative of turbulence, since we expect turbulent fields to display little to no symmetry in general. As a result, while the symmetric exact coherent structures appear to inform our understanding of turbulent transitions, they do not necessarily inform our understanding of turbulent dynamics. The focus of this thesis has been to investigate the properties of periodic orbits with broken symmetry, and their relation to structures in symmetric spaces.

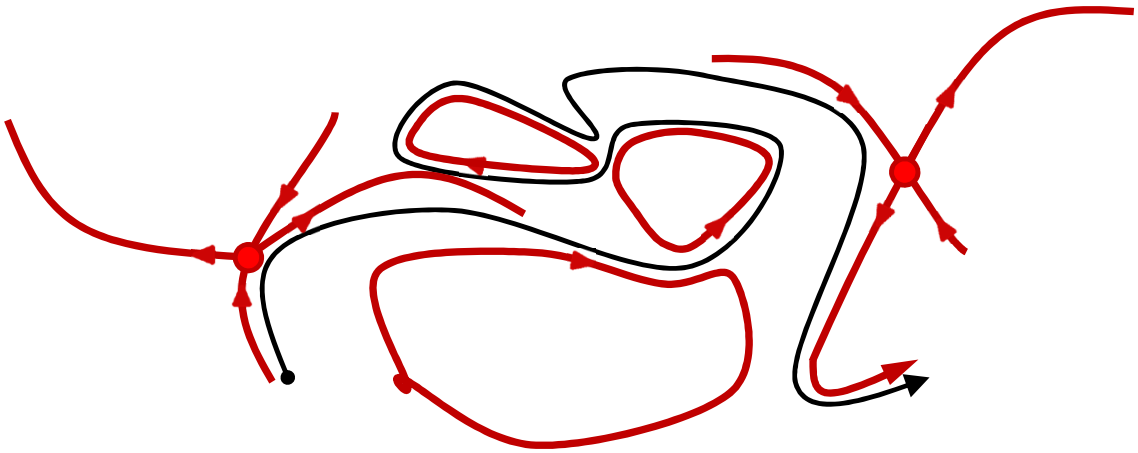

Figure 7: A turbulent trajectory in black appears chaotic in isolation, but is in fact guided by exact coherent structures of the flow.

In the first chapter, I will lay out in further detail the Navier-Stokes equation and problem geometry. In the second chapter, I will discuss the symmetries of the Navier-Stokes equations for plane Couette flow, and the advantges and disadvantages afforded by considering symmetric subspaces. The third chapter will discuss in detail the spectral methods used to integrate Navier-Stokes forward in time and the Newton-Krylov-hookstep algorithm used to find coherent structures in Channelflow, along with the workflow used in this thesis. Chapter 4 presents the results of this thesis, which includes low period reduced symmetry orbits over a large range of Reynolds numbers. Chapter 5 will then summarize this thesis, and suggest potential topics for future research.

Chapter 1

Equations of Flow

For every action, there is an equal and opposite regulatory body

Anonymous

1.1 Formalisms

If we were considering the dynamics of a point particle, we would begin with Newton's Second Law -

$$\frac{\mathrm{d}\mathbf{p}}{\mathrm{d}t} = \mathbf{F}, \tag{1.1}$$

write down the body force as a function of position, time, etc., and have our differential equation. The solution may be found analytically or numerically, but is nevertheless trivial. While we can in principle use this approach to describe the behavior of a large collection of particles making up the fluid, practical considerations prevent us from modeling the behavior of each individual particle, for the following reason – in a milliliter of water, there are approximately 10^{22} molecules of water, each with 6 degrees of freedom[1]. Applying (1.1) to all these particles would result in about 10^{23} coupled partial differential equations. Such a set of equations would be hard to write down, let alone solve! Clearly, a more intelligent approach is needed.

1.1.1 The Eulerian Formulation

When asked to consider the mechanical evolution of some collection of bodies, two obvious methods would be readily apparent - we could either follow a collection of particles on their way through space and time (the **Lagrangian** formulation), or we could situate ourselves at some point in space and observe the properties of particles that pass through the surrounding region (the **control volume**) over time

[1] If we ignore the vibrations of the O-H bonds

(the **Eulerian** formulation). The Lagrangian formulation will be familiar to anyone with a basic physics education, since it lends itself readily towards analysis of rigid-body motion. When considering fluids, however, the disadvantages of the Lagrangian formulation (noted above) stand in contrast to the ease of analysis afforded by the Eulerian formulation, which remains as easy (or hard) as it was for rigid body motion. For this reason, I will focus on the Eulerian formulation of fluid mechanics in this thesis.

1.1.2 The Fluid Particle

As a consequence of the Eulerian formulation, we cannot know the full timeline of any individual particle over its lifetime – we only know the properties of particles within the control volume. Therefore, the principle quantity of consideration for the Eulerian formulation is the velocity field[2] $\mathbf{v}(\mathbf{x},t) = v_x(\mathbf{x},t)\hat{\mathbf{x}} + v_y(\mathbf{x},t)\hat{\mathbf{y}} + v_z(\mathbf{x},t)\hat{\mathbf{z}}$, along with the pressure and density fields, which are the average values of the property in a control volume surrounding a point. A subtle issue arises in doing this, however. Since the velocity field is continuous, it has a well defined value at every point in space, which we would want to be associated with the velocity of a particle at that point in space. But there are finite number of particles in any collection of fluid with a finite spatial extent - so it would appear that the formulation assigns multiple different velocities to a single particle! The resolution to this is the continuum hypothesis, which suggests that the control volume (the '**fluid parcel**') can be chosen such that it is large enough to form a meaningful average of the quantities within, but small enough that the properties do not vary significantly over the parcel, and that from a macroscopic perspective, the properties appear continuous. The reader may ask "Can such a parcel even exist?". As an example to such a reader, let us consider water, with approximately 10^{22} molecules per cubic centimeter. Imagine our fluid parcels as cubes filling up space, with sides of length dl, giving a total volume of dl^3. First, let us make dl small enough that the macroscopic properties appear continuous - how about one micron? That gives the volume of a fluid particle as one cubic micrometer. For scale, consider that the volume of the human red blood cell ranges from 80-100 cubic micrometers[21] - this seems acceptably small for considering, say, the flow around a ship.[3] The number of water molecules within each fluid parcel is then

$$10^{22} dl^3 = 10^{22} \times 10^{-12} = 10^{10}, \tag{1.2}$$

or about 10 billion water molecules, which is certainly sufficient to achieve a meaningful average. Having defined a fluid parcel in this way allows us to behave as if these external variables have well defined values at every point in space, which greatly simplifies the following analysis.

[2] As opposed to particle trajectories $\mathbf{x}(t)$ in the Lagrangian formulation.

[3] The validity of the continuum hypothesis is clearly dependent on the density of the fluid and the length scale of the phenomenon to be modeled, but holds up even for the sparse gas clouds of protoplanetary disks

1.2 Mass Conservation

While not technically a part of the Navier-Stokes equation (which is a statement about conservation of linear momentum), conservation of mass is nevertheless essential in solving fluid problems, and will serve as an easy demonstration of the control volume principle. Consider a volume Ω which is fixed in space, and has some mass density $\rho = \rho(\mathbf{x}, t)$ and some fluid velocity $\mathbf{v} = \mathbf{v}(\mathbf{x}, t)$ that are generically functions of time and space, allowing us to define the **mass current density** $\mathbf{m} = \mathbf{v}\rho$. We would prefer that our equations not allow mass to disappear (excluding high-energy physics, naturally), and would additionally prefer a mathematical form of this statement.

The mass contained within the volume Ω is given by

$$M = \int_\Omega \rho \ dV. \tag{1.3}$$

The flow of mass out of the volume through the surface $d\Omega$ of Ω is given by

$$\mathcal{M}_{flow} = \int_{d\Omega} \mathbf{m} \cdot \mathbf{n} \ dA = \int_\Omega \nabla \cdot (\rho \mathbf{v}) \ \ dV, \tag{1.4}$$

by the divergence theorem. Now if mass is conserved, the sum of the rate of mass flow into (or out of) the volume and the rate of change of mass inside the volume must be zero, giving

$$\frac{\partial M_{encl}}{\partial t} + \mathcal{M}_{flow} = 0, \tag{1.5}$$

$$\frac{\partial}{\partial t}\left(\int_\Omega \rho \ dV\right) + \int_\Omega \nabla \cdot (\rho \mathbf{v}) \ \ dV = 0, \tag{1.6}$$

but since Ω is time independent, the time derivative commutes with the integral, giving

$$\int_\Omega \frac{\partial \rho}{\partial t} + \nabla \cdot (\rho \mathbf{v}) \ \ dV = 0. \tag{1.7}$$

Since Ω is arbitrary, the integrand must be zero everywhere, so mass is conserved if

$$\frac{\partial \rho}{\partial t} + \nabla \cdot (\rho \mathbf{v}) = 0. \tag{1.8}$$

Now, (1.8) can be expanded further by using the chain rule for divergence, giving

$$\frac{\partial \rho}{\partial t} + \rho \nabla \cdot \mathbf{v} + \mathbf{v} \nabla \rho = 0. \tag{1.9}$$

If the flow is (approximately) incompressible, which will be true for small Mach numbers[4], then ρ must be constant, and (1.9) becomes

$$\nabla \cdot \mathbf{v} = 0, \tag{1.10}$$

for both steady and unsteady flows.

[4]The Mach number is the ratio of the fluid velocity to the speed of sound in the fluid. For reference, the speed of sound in water is 1497 ms^{-1} at room temperature and pressure.

1.3 Conservation of Linear Momentum

As mentioned earlier, the Navier-Stokes equations are simply a statement of conservation of linear momentum, along with certain assumptions about stress and strain, which are presented below.

1.3.1 Stress

Stress contains information about the forces on an object. As with force, we define positive stress as stress that acts towards the control volume, and negative if they act away. Unlike force, stress objects are not vectors. Not only do they have a magnitude and direction, but they also have a plane that they act from. Since there are three directions and three planes of action, stress objects generally have nine elements, and are **second rank tensors**. For example, the viscous stress tensor $\mathcal{T}$ is identified by two subscripts, where the first subscript indicates the plane of action, and the second the direction of action. So $\mathcal{T}_{xy}$ would represent the viscous force on the (y, z) plane acting in the y direction. Note than in a Cartesian coordinate system, a second rank tensor can be written as a matrix.

1.3.2 Strain

Now that we can consider the forces on a fluid particle, we need to link these forces back to the observable quantities[5]. In solids, this is easy - Hooke's Law for elastic substances, for instance, sets the strain proportional to the stress:

$$\sigma = \mathcal{C}\epsilon, \tag{1.11}$$

where σ is the Cauchy stress tensor, $\mathcal{C}$ is the (fourth rank) stiffness tensor and ϵ is the infinitesimal strain tensor. However, for fluids, this is not the case - you can imagine that if you applied a constant force to a cube of water, it would deform continuously, without offering any resistance. Newton theorized that for continuously deformable fluids, the 1-D relationship between stress $\mathcal{T}$ and strain $\mathcal{S}$ should have the following form:

$$\mu\frac{\mathrm{d}\mathcal{S}}{\mathrm{d}t} = \mu\frac{\mathrm{d}u}{\mathrm{d}x} = \mathcal{T}, \tag{1.12}$$

where μ is the fluid viscosity and u is the velocity. Stokes extended this to three dimensions, giving the Newtonian constitutive relationship between stress and strain (for an incompressible fluid):

$$\mathcal{T}_{ij} = -P\delta_{ij} + \mu\left(\frac{\partial u_i}{\partial x_j} + \frac{\partial u_j}{\partial x_i}\right), \tag{1.13}$$

where δ_{ij} is the Kronecker delta function[6] and P is the pressure. A fluid obeying Newton's constitutive relation is called a Newtonian fluid. Water, and most gases under normal conditions are Newtonian, but fluids like blood, quicksand and corn starch (to name a few) are not.

[5] Deformations in solids and velocity fields in fluids

[6] $\delta_{ij} = 1$ if $i = j$ and 0 otherwise

1.3.3 Surface Forces

Having written down the stress tensor $\mathcal{T}$ as a function of the velocity field, we can now link it to the surface forces on a fluid particle. Recalling that stresses act over $d\Omega$ of the fluid particle, the total force is then simply

$$\mathbf{F} = \int_{d\Omega} \mathcal{T} \cdot \mathbf{n} \; dA, \tag{1.14}$$

where $\mathbf{n}$ is the surface normal.

1.3.4 Newton's Second Law

For a fluid parcel Ω, Newton's Second Law can be rewritten as

$$\sum \mathbf{F} = \int_{\Omega} \frac{\partial \mathbf{p}}{\partial t} \; dV \tag{1.15}$$

where the sum is over all possible external forces. We can further split $\mathbf{F}$ into two kinds of forces - body forces, like gravity or electromagnetism, and surface forces due to stress. We group the body forces $\mathbf{F}_b$ as

$$\mathbf{F}_b = \int_{\Omega} \rho \mathbf{f} \; dV, \tag{1.16}$$

where $\mathbf{f}$ is the **body force density**. Using (1.14) to express the surface forces, Newton's Second Law becomes

$$\int_{\Omega} \rho \mathbf{f} - \frac{\partial \mathbf{p}}{\partial t} \; dV + \int_{d\Omega} \mathcal{T} \cdot \mathbf{n} \; dA = 0, \tag{1.17}$$

which can be written in differential form by the same trick used to generate (1.8), giving Cauchy's Equation of Motion

$$\rho \mathbf{f} - \frac{\partial \mathbf{p}}{\partial t} + \nabla \cdot \mathcal{T} = 0. \tag{1.18}$$

From this, the incompressible Navier-Stokes equation arise by a substitution of (1.13) into (1.18), giving (after tedious rearrangement by components),

$$\frac{\partial \mathbf{u}}{\partial t} + (\mathbf{u} \cdot \nabla)\, \mathbf{u} = \mathbf{f} - \frac{1}{\rho} \nabla P + \frac{\mu}{\rho} \nabla^2 \mathbf{u}. \tag{1.19}$$

By using the substitutions

$$\mathbf{x} \Rightarrow L\mathbf{x} \tag{1.20}$$

$$\mathbf{u} \Rightarrow U\mathbf{u} \tag{1.21}$$

$$t \Rightarrow \frac{L}{U} t \tag{1.22}$$

$$P \Rightarrow \rho U^2 P, \tag{1.23}$$

and neglecting body forces, we obtain the nondimensional version of (1.19) –

$$\frac{\partial \mathbf{u}}{\partial t} + (\mathbf{u} \cdot \nabla)\,\mathbf{u} = -\nabla P + \frac{1}{Re}\nabla^2 \mathbf{u}, \tag{1.24}$$

$$\nabla \cdot \mathbf{u} = 0, \tag{1.25}$$

where

$$Re = \frac{UL\rho}{\mu}. \tag{1.26}$$

In practice, the values of L and U are chosen by convention to reflect the natural scales of the problem at hand.

1.4 Plane Couette Flow

The Navier-Stokes equation for plane Couette flow is given by

$$\frac{\partial \mathbf{u}}{\partial \tau} + (\mathbf{u} \cdot \nabla)\,\mathbf{u} = \frac{1}{Re}\nabla^2 \mathbf{u}, \tag{1.27}$$

with geometry as pictured in Figure 2. We nondimensionalize by the velocity V of either plate and the half-plate distance h, with the Reynolds number

$$Re = \frac{hV\rho}{\mu}. \tag{1.28}$$

Since plane Couette flow is a shear driven flow, we set the pressure gradient to zero and use no slip boundary conditions at the walls, which sets the surface tangential velocity equal to the surface velocity. In order to derive the laminar velocity profile shown earlier in Figure 3, note that at very low Re, the right hand side of (1.27) dominates. If we assume that the flow is unidirectional and steady, so that $\mathbf{u} = u_x \hat{\mathbf{x}}$, and note that by symmetry considerations, the velocity field can only be a function of height, the Navier-Stokes equation reduces to

$$\frac{\partial^2 u_x}{\partial y^2} = 0, \tag{1.29}$$

with no-slip boundary conditions

$$u(-1) = -1, \tag{1.30}$$

$$u(1) = 1. \tag{1.31}$$

This has a solution of the form

$$\mathbf{u}(y) = y\hat{\mathbf{x}}, \tag{1.32}$$

which corresponds to the laminar flow profile in Figure 3. Consider then a perturbation $\mathbf{v}(x, y, z, t)$ from this laminar state, so that the initial field is $\mathbf{u}(x, y, z, t) = \mathbf{v}(x, y, z, t) + y\hat{\mathbf{x}}$. Substituting this into (1.24), we get

$$\frac{\partial \mathbf{v}}{\partial \tau} + y\frac{\partial \mathbf{v}}{\partial x} + v\hat{\mathbf{x}} + \mathbf{v} \cdot \nabla\,\mathbf{v} = \frac{1}{Re}\nabla^2 \mathbf{v}, \tag{1.33}$$

$$\nabla \cdot \mathbf{v} = 0, \tag{1.34}$$

with the no-slip boundary conditions

$$\mathbf{v}(x, \pm 1, z, t) = 0. \tag{1.35}$$

In addition, artificial boundary conditions must be imposed to treat the infinite domain, which is computationally intractable otherwise. The periodic boundary conditions

$$\mathbf{v}(x, y, z, t) = \mathbf{v}(x + L_x, y, z, t), \tag{1.36}$$
$$\mathbf{v}(x, y, z, t) = \mathbf{v}(x, y, z + L_z, t), \tag{1.37}$$

are used, where L_x and L_z are the lengths of the periodic cell. This gives the complete equation of motion for the perturbing velocity field. Since the laminar profile is steady, understanding the turbulent field's trajectory in state space now reduces to understanding the behavior of the turbulent perturbation, and the structure of its inertial manifold.

Chapter 2

Symmetry in plane Couette flow

Tyger! Tyger! Burning bright,
In the forests of the night.
What immortal hand or eye,
Could frame thy fearful symmetry?

William Blake, *The Tyger*

Dynamical systems in physics often display symmetry. The electron wavefunction in the ground state of hydrogen, or the gravitational motion of a planet around a star, for instance, display very high degrees of spatial symmetry. Understanding the symmetries of a system can be incredibly useful to an investigator, since they hint at conserved physical quantities (through Noether's Theorem), and can greatly reduce the complexity of the system in various ways. Before I begin the discussion of the symmetries of plane Couette flow, I will first define what 'symmetry' means in this thesis. A system is said to be **equivariant** under a symmetry transformation of the dynamical system if the transformation commutes with the time evolution of the system - that is, for a symmetry transformation S and a dynamical system $\dot{x} = f(x)$,

$$S\dot{x} = Sf(x) = f(Sx). \tag{2.1}$$

The symmetry relations of plane Couette flow are discussed extensively in [22], which I will present here for the sake of flow[1].

2.1 Unbounded Navier-Stokes

If we do not impose boundary conditions on the Navier-Stokes equations on an infinite domain, the system will be equivariant under continuous rotational and translational symmetry, as well as the discrete **pointwise inversion** symmetryσ_{xz}, which has the following action on the system:

$$\sigma_{xz}\mathbf{u}(\mathbf{x}) = -\mathbf{u}(-\mathbf{x}) \tag{2.2}$$

[1] haha

While the rotation or translation transformation can be easily conceptualized, the pointwise inversion can provide some difficulty. The easiest way of visualizing the transformation is to view it in a 2D domain instead of in the full 3D, as shown in Figure 2.1. The proof of the equivariance of Navier-Stokes under these transformations can be found in [23].

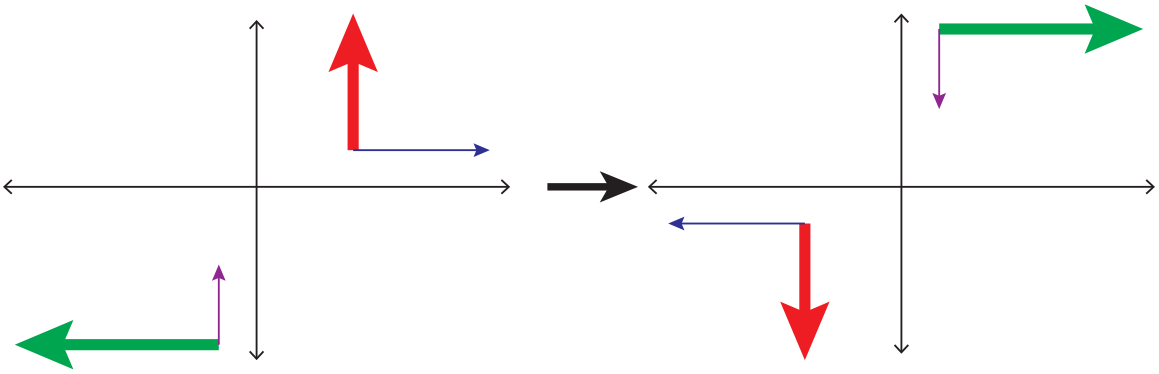

Figure 2.1: A 2D pointwise inversion operation on two sets of vectors according to (2.2).

2.2 Plane Couette Flow

If the domain is limited to $\mathbb{R}^2 \times [-1, 1]$ with the boundary conditions of plane Couette flow, we lose some of the equivariant transformations of the full, unrestricted problem, leaving us with two basic discrete symmetries: a rotation by π about the z axis (denoted σ_x) and a reflection about the z axis (denoted σ_z)[2], together form a discrete symmetry group $D = D_1 \times D_1 = \{e, \sigma_x, \sigma_z, \sigma_{xz}\}$ of order 4, where

$$\sigma_x[u, v, w](x, y, z) = [-u, -v, w](-x, -y, z) \tag{2.3}$$
$$\sigma_z[u, v, w](x, y, z) = [u, v, -w](x, y, -z) \tag{2.4}$$
$$\sigma_{xz}[u, v, w](x, y, z) = [-u, -v, -w](-x, -y, -z) \tag{2.5}$$

The continuous symmetries are the two parameter steamwise-spanwise translations, which, when provided periodic boundary conditions, form a continuous $SO(2) \times SO(2)$ symmetry group

$$\tau(l_x, l_z)[u, v, w](x, y, z) = [u, v, w](x + l_x, y, z + l_z). \tag{2.6}$$

The group Γ of equivariant solutions is then any combination of these symmetry operations, given by $\Gamma = SO(2)_x \ltimes D_{1,x} \times SO(2)_z \ltimes D_{1,z}$[3]. For a solution $\mathbf{u}$ of plane Couette flow, the group s of symmetries that satisfies $s\mathbf{u} = \mathbf{u}$ is called the isotropy

[2]The motivation for these subscripts will become apparent shortly
[3]$\ltimes$ is the semidirect product

subgroup of $\mathbf{u}$ and is said to fix $\mathbf{u}$. Examples of such groups include the identity group $\{e\}$, which is typically the isotropy subgroup of turbulent solutions. Before I discuss the isotropy subgroup considered for this thesis, however, I will first highlight the useful properties of some particular symmetry subgroups to motivate the eventual choice of isotropy subgroup.

2.3 Properties of Γ

It should be evident that since plane Couette flow is equivariant under the continuous translations given in (2.6), trajectories can be traveling wave equilibria or relative periodic orbits: that is, if one moves into a different reference frame, the trajectory is a regular equilibrium or periodic orbit. However, an initial condition that is fixed by σ_z cannot be translated in the spanwise direction without losing σ_z symmetry (except for the trivial case where $\frac{\partial \mathbf{u}_z}{\partial z} = 0$). Similarly, an initial condition that is fixed by σ_x cannot be translated in the streamwise direction without losing σ_x symmetry (and an initial condition that is fixed by σ_{xz} symmetry cannot be translated at all without losing σ_{xz} symmetry). Since these symmetries are also invariant[4], a trajectory with one of the discrete symmetries cannot be a traveling wave in the direction corresponding to its subscript.

The presence of the periodic boundary conditions also implies that all solutions are fixed by the full-period translation $\tau(L_x, 0)$ and $\tau(0, L_z)$. However, solutions can also be fixed by any rational translation of the form $\tau(aL_x, bL_z)$, where $a, b \in \mathbb{Q}$, or by the continuous translations. If we fix $\mathbf{u}$ by a continuous translation, we force it to have a zero derivative along that axis[5], and such solutions tend to be uninteresting as they are equivalent to low-dimensional problems. If $\mathbf{u}$ is fixed instead by rational translations, the periodic cell is tiled with repeating subcells , as in Figure 2.2. This implies that we can restrict ourselves to full box length translations, which are in any case required by the periodic boundary conditions.

Finally, we can reduce the number of unique subgroups of Γ by considering its **conjugacy groups**. A group N and M are considered conjugate if for some $s \in \Gamma$, $N = s^{-1}Ms$ - that is, N and M are related by a coordinate transformation. This allows us to consider only one group out of a set of mutually conjugate groups (known as a conjugacy class), since any other group in the class is simply related by the application of a symmetry transformation. This becomes especially important when considering $O(2) = SO(2) \ltimes D_1$, since it is not an abelian group as reflections and translations about the same axis are noncommutative (Figure 2.3). However, we can still recover a psuedo-commutative relation by considering Figure 2.4. We can see that $\sigma_z \tau_z$ results in the object moving by l_z to the right, and the being mirrored across the z axis, at which point it is mirrored and l_z to the left of the origin. We

[4]That is, if the symmetry is satisfied at time $t = t_0$, it must be satisfied for all times.

[5]That is, if we fix $\mathbf{u}$ by $\tau l_x, 0$ for any real l_x, then $\frac{\partial \mathbf{u}}{\partial x} = 0$, and similarly for z.

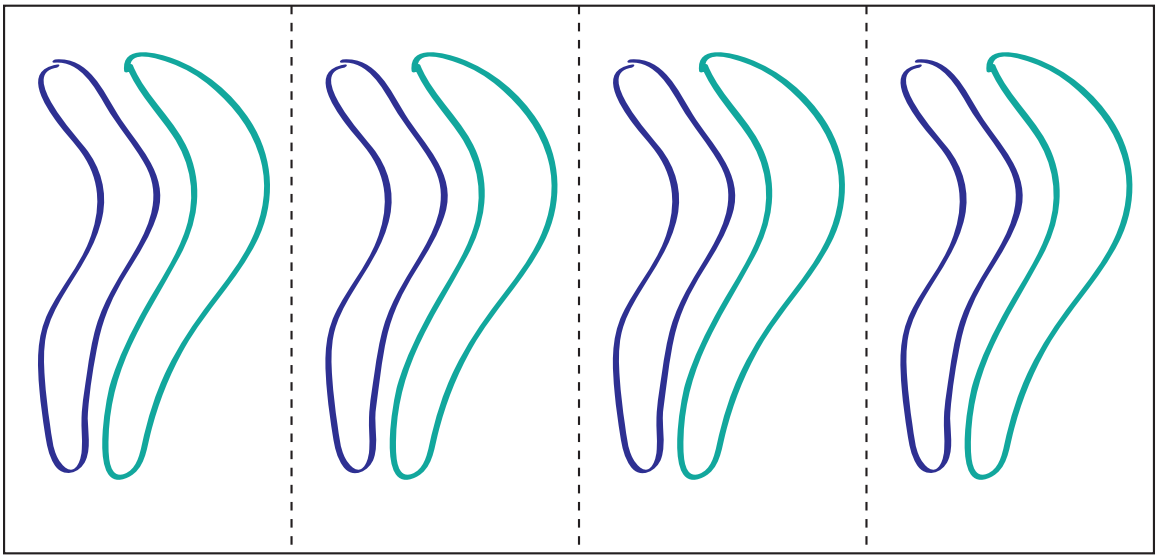

Figure 2.2: If the flow state is fixed by $\tau(\frac{1}{4}L_x, 0)$, then the cell will have four repeating streamwise subcells, and it becomes more efficient to solely consider the subcell.

can achieve the same effect by mirroring the object and moving it to the left - that is, applying the operation $\tau_z^{-1}\sigma_z$, leading us to conclude that $\sigma\tau = \tau^{-1}\sigma$. We can rewrite this as $\sigma\tau^2 = \tau^{-1}\sigma\tau$, so

$$\sigma_x\tau(l_x, 0) = \tau^{-1}(l_x/2, 0)\sigma_x\tau(l_x/2, 0), \tag{2.7}$$

which implies that σ_x and $\sigma_x\tau_x$ are part of the same conjugacy class - so if a isotropy group contains $\sigma_x\tau_x$, there is a simpler version of that group which contains σ_x instead. Note that if $l_x = L_x$, then we have $\sigma_x = \tau_x^{-1}\sigma_X\tau_x$, so reflection and translations commute for any half-integer cell shifts. In this thesis, I will work with either half-cell or or null shifts. The group of half cell shifts is denoted C_2, so the group

$$G = D_{1,x} \times C_{2,x} \times D_{1,z} \times C_{2,z} \subset \Gamma \tag{2.8}$$

is an abelian group of order 16, containing both the isotropy groups of half-cell and null shifts.

2.4 Symmetry Groups of this Thesis

We can categorize the conjugacy classes of G by their order - in this thesis, we will work with order 2 and 4 classes. There are 15 subgrups of order-2 (since there are 15 non-identity elements in G), 35 subgroups of order 4 ($(15 \cdot 14)/(3 \cdot 2)$), 15 subgroups of order 8 and 1 subgroup of order 16, giving 67 subgroups of G. Luckily, the existence of conjugacy classes allow us to greatly simplify the number of distinct groups we need to consider. For order-2 subgroups, conjugacy between σ_x and $\sigma_x\tau_x$

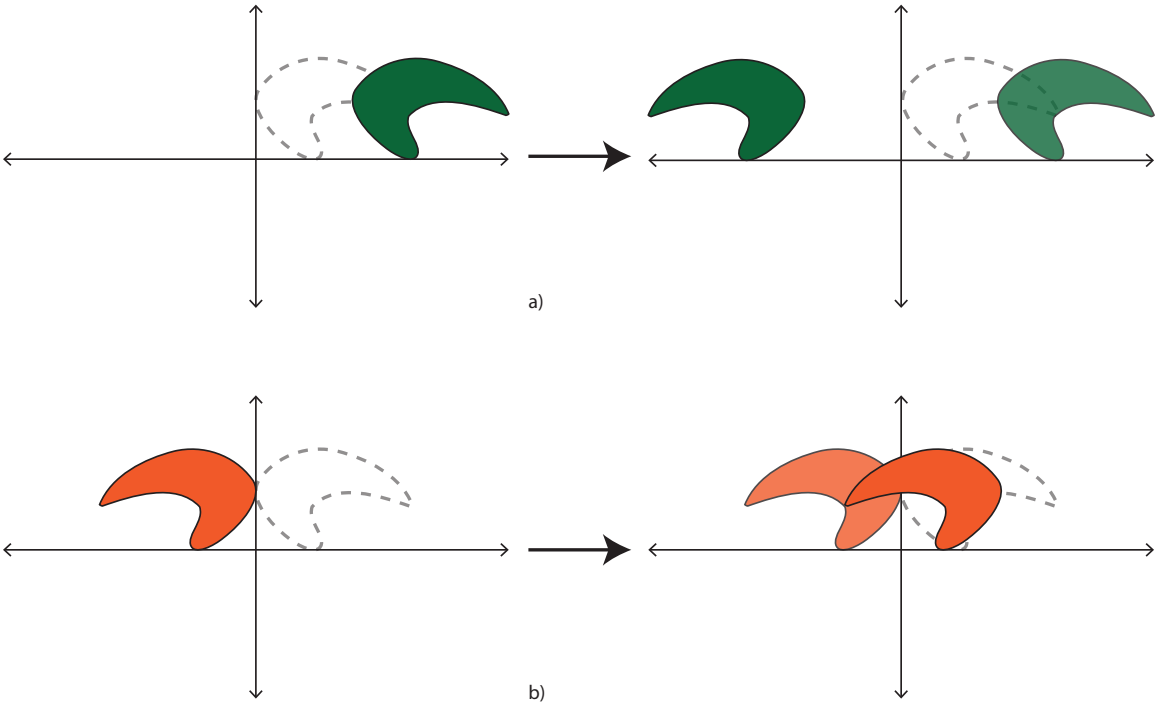

Figure 2.3: A simple demonstration that shifts and reflects do not commute in general. a) shows an object with a dashed outline that is translated to the right, and then reflected across the vertical, while b) shows the same object reflected before it is translated to the right. Notice that the final positions of the object are not the same.

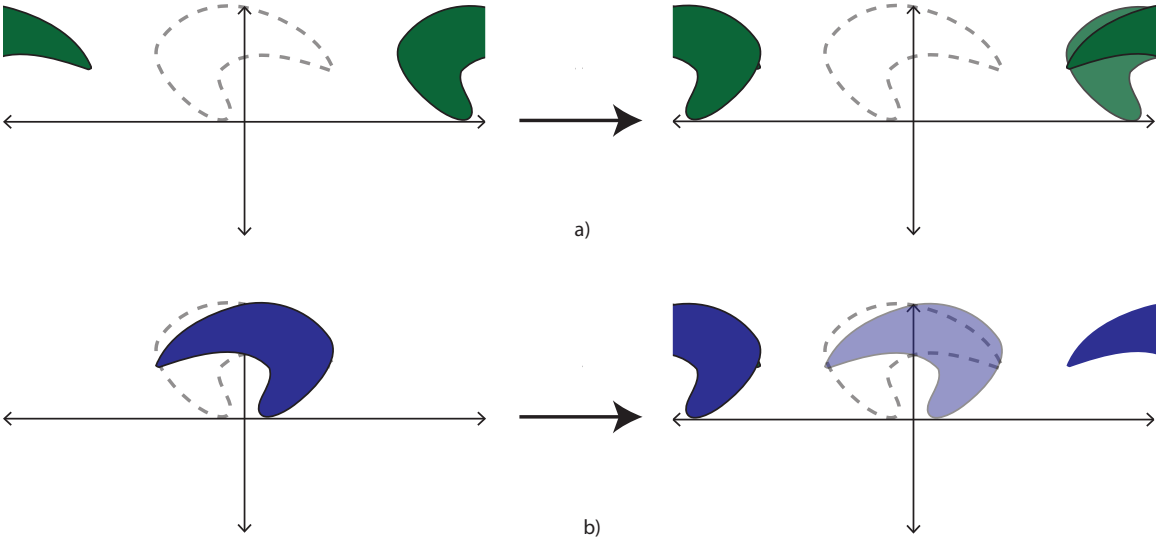

Figure 2.4: When periodic boundary conditions are imposed and translations are fixed to half-period lengths, shifts and reflects commute. a) shows an object that is shifted and then reflected across the vertical, while b) shows the same object reflected across the vertical and then shifted. Notice that the final positions are the same, even if the indermediaries are not.

and $\sigma_z\tau_z$ allows us to simplify down to just 8 distinct groups, which are generated by $\sigma_x, \sigma_z, \sigma_{xz}, \sigma_x\tau_z, \sigma_z\tau_x, \tau_x, \tau_z, \tau_{xz}$. Recalling the behavior of these symmetries, we can see that only σ_{xy} generates a group without travelling waves, σ_z and $\sigma_z\tau_x$ generate groups that allow travelling waves in the x direction, $\sigma_x\tau_z$ and $\sigma_x\tau_z$ generate groups that allow travelling waves in the z direction, and the pure translations allow travelling waves in any (in-plane) direction.

Chapter 3

Numerics and Workflow

> On two occasions I have been asked, "Pray, Mr. Babbage, if you put into the machine wrong figures, will the right answers come out?" ... I am not able rightly to apprehend the kind of confusion of ideas that could provoke such a question.
>
> Charles Babbage, Passages from the Life of a Philosopher

Computational studies of Navier-Stokes, especially as a dynamical system is difficult for many reasons, but most important among them is the high degree of complexity inherent in the numerical tools required to efficiently simulate it. As mentioned earlier, the two major approaches towards simulating Navier-Stokes is modelling, where some assumptions are made to reduce the difficult of simulation, and direct numerical simulation (DNS), where no assumptions beyond those used to derive Navier-Stokes and set up the boundary conditions are used. DNS is naturally more accurate (since the physicality of some modelling assumptions can be suspect), but since it fully resolves Navier-Stokes, it is significantly more expensive than modeling, and methods that attempt to offset this extra cost tend to be extremely complex. For this reason, I use the open source library `Channelflow` [20], which has been essential in making any headway in this thesis. `Channelflow` is a spectral DNS library, with additional utilities to find, parametrically continue, and analyze exact coherent structures, which I will lay out in some detail below.

3.1 The Spectral Method

3.1.1 The Residual

Spectral methods are, like finite element methods, part of a larger class of numerical methods known as **weighted residual methods**. In this class of methods, functions

are approximated by a truncated series expansion, with the restriction that a quantity related to the residual be zero (instead of the residual itself). The quantity used for the sprectral method is the scalar product

$$\langle u, v \rangle_w = \int_a^b uvw \ dx, \tag{3.1}$$

where $u(x), v(x)$ are some functions on the interval $[a, b]$, and $w(x)$ is a weighting function. If we then imagine some platonic function[1] $u(x)$ that we attempt to approximate via a finite series expansion, so that

$$u_N(x) = \sum_{k=0}^{N} \hat{u}_k \psi_k(x), \tag{3.2}$$

for some set of orthogonal basis functions $\psi_k(x)$, then the residual is given by

$$R_N = u(x) - u_N(x), \tag{3.3}$$

and for some differential equation

$$Du = f, \tag{3.4}$$

where D is some arbitrary differential operator and $f(x)$ is some arbitrary source function, the residual is defined

$$R_N = Du_N, \tag{3.5}$$

as expected. While it may seem logical to require $R_N = 0$, this is not possible in general for finite N, so we instead require

$$\langle R_N, \delta(x - x_i) \rangle_1 = R_N(x_i) = 0, \tag{3.6}$$

for some set of x_i. This method of minimizing the residual is known as the collocation method, has the effect of forcing the series expansion to match the platonic function at some set of points.[2] In the spectral method, the basis functions are trignometric functions. The advantage of trignometric functions over polynomials is the rapid convergence of the series coefficients – the Fourier coefficients converge exponentially fast, so we can achieve extremely high accuracy with a lower number of modes [24].[3] `Channelflow` uses Fourier series, where the basis functions are given by

$$F_k(x) = \exp ikx, \tag{3.7}$$

and Chebyshev polynomials of the first kind, where the basis functions satisfy

$$T_k(x) = \cos(k \arccos x). \tag{3.8}$$

[1] That is, the function that is to be approximated

[2] The other popular method of minimizing the residual, the Galerkin method, sets the mean residual as zero

[3] Spectral methods are inappropriate when the boundary geometry is highly complex, as is the case in the majority of industrial applications, where more general finite element methods are used.

The Fourier series expansion is particularly nice since the derivative $\partial_x F_k(x) = ikF(x)$. To see how the spectral method is applied to solving nonlinear partial differential equations, consider the 1D Swift-Hohenburg equation

$$\frac{\partial u}{\partial t} = \kappa u - \left(1 + \frac{\partial^2}{\partial x^2}\right)^2 u - u^2. \tag{3.9}$$

Expanding (3.9), we get

$$\frac{\partial u}{\partial t} = (\kappa - 1)\, u - 2\frac{\partial^2 u}{\partial x^2} - \frac{\partial^4 u}{\partial x^4} - u^2. \tag{3.10}$$

If we assume a Fourier series approximation to u, and denote the approximation at time $n\Delta t$ by $u_K^n(x)$, then using a forward-difference method to discretize (3.10), we get the residual

$$R_K = \frac{u_K^{n+1} - u_K^n}{\Delta t} + (\kappa - 1)u_K^n \tag{3.11}$$

While Fourier expansions are the easiest to deal with, they are best used on periodic boundaries, since the imposition of aperiodic boundary conditions on a Fourier series expansion can lead to Gibbs oscillations that can make the simulation aphysical [24]. For this reason, the velocity field is expanded as a Fourier series in the plane, and as a Chebyshev polynomial in the wall-normal direction. The velocity field is then represented as

References

[1] S. Taneda, "Experimental investigation of the wake behind a sphere at low reynolds numbers," *Journal of the Physical Society of Japan*, vol. 11, no. 10, pp. 1104–1108, 1956.

[2] B. Eckhardt, H. Faisst, A. Schmiegel, and T. M. Schneider, "Dynamical systems and the transition to turbulence in linearly stable shear flows," *Philosophical Transactions of the Royal Society of London A: Mathematical, Physical and Engineering Sciences*, vol. 366, no. 1868, pp. 1297–1315, 2008.

[3] P. Manneville, "On the transition to turbulence of wall-bounded flows in general, and plane Couette flow in particular," *European Journal of Mechanics B Fluids*, vol. 49, pp. 345–362, Jan. 2015.

[4] U. Brosa, "Turbulence without strange attractor," *Journal of Statistical Physics*, vol. 55, no. 5-6, pp. 1303–1312, 1989.

[5] B. Hof, A. de Lozar, D. J. Kuik, and J. Westerweel, "Repeller or attractor? selecting the dynamical model for the onset of turbulence in pipe flow," *Phys. Rev. Lett.*, vol. 101, p. 214501, Nov 2008.

[6] S. Bottin and H. Chaté, "Statistical analysis of the transition to turbulence in plane couette flow," *The European Physical Journal B-Condensed Matter and Complex Systems*, vol. 6, no. 1, pp. 143–155, 1998.

[7] F. Daviaud, J. Hegseth, and P. Bergé, "Subcritical transition to turbulence in plane couette flow," *Phys. Rev. Lett.*, vol. 69, pp. 2511–2514, Oct. 1992.

[8] S. Pope, *Turbulent Flows*. Cambridge University Press, 2000.

[9] E. Hopf, "A mathematical example displaying features of turbulence," *Commun. Pure Appl. Math.*, vol. 1, no. 4, pp. 303–322, 1948.

[10] C. Foias, G. R. Sell, and R. Temam, "Inertial manifolds for nonlinear evolutionary equations," *Journal of Differential Equations*, vol. 73, no. 2, pp. 309–353, 1988.

[11] P. Grassberger and I. Procaccia, "Measuring the strangeness of strange attractors," in *The Theory of Chaotic Attractors*, pp. 170–189, Springer, 2004.

[12] E. N. Lorenz, "Deterministic nonperiodic flow," *Journal of the atmospheric sciences*, vol. 20, no. 2, pp. 130–141, 1963.

[13] N. Aubry, P. Holmes, J. L. Lumley, and E. Stone, "The dynamics of coherent structures in the wall region of a turbulent boundary layer," *Journal of Fluid Mechanics*, vol. 192, pp. 115–173, 7 1988.

[14] O. Dauchot and N. Vioujard, "Phase space analysis of a dynamical model for the subcritical transition to turbulence in plane couette flow," *The European Physical Journal B-Condensed Matter and Complex Systems*, vol. 14, no. 2, pp. 377–381, 2000.

[15] M. Nagata, "Three-dimensional finite-amplitude solutions in plane couette flow: bifurcation from infinity," *J. Fluid Mech.*, vol. 217, pp. 519–527, 1990.

[16] F. Waleffe, "Exact coherent structures in channel flow," *Journal of Fluid Mechanics*, vol. 435, pp. 93–102, 5 2001.

[17] G. Kawahara and S. Kida, "Periodic motion embedded in plane couette turbulence: regeneration cycle and burst," *J. Fluid Mech.*, vol. 449, pp. 291–300, 2001.

[18] D. Viswanath, "Recurrent motions within plane couette turbulence," *J. Fluid Mech.*, vol. 580, pp. 339–358, 2007.

[19] J. F. Gibson, J. Halcrow, and P. Cvitanović, "Visualizing the geometry of state space in plane couette flow," *Journal of Fluid Mechanics*, vol. 611, pp. 107–130, 2008.

[20] J. F. Gibson, "Channelflow: A spectral Navier-Stokes simulator in C++," tech. rep., U. New Hampshire, 2014. `Channelflow.org`.

[21] S. L. Fischer and S. P. Fischer, "Mean corpuscular volume," *Archives of Internal Medicine*, vol. 143, no. 2, pp. 282–283, 1983.

[22] J. F. Gibson, J. Halcrow, and P. Cvitanovic, "Equilibrium and travelling-wave solutions of plane couette flow," *Journal of Fluid Mechanics*, vol. 638, pp. 243–266, Nov. 2009.

[23] V. Gusyatnikova and V. Yumaguzhin, "Symmetries and conservation laws of navierstokes equations," in *Symmetries of Partial Differential Equations*, pp. 65–81, Springer, 1989.

[24] R. Peyret, *Spectral methods for incompressible viscous flow*, vol. 148. Springer Science & Business Media, 2002.

[25] T. v. Karman, "Mechanische aenlichkeit und turbulenz," *Nachrichten von der Gesellschaft der Wissenschaften zu Gttingen, Mathematisch-Physikalische Klasse*, vol. 1930, pp. 58–76, 1930.

[26] A. N. Kolmogorov, "The local structure of turbulence in incompressible viscous fluid for very large reynolds numbers," *Proceedings of the Royal Society of London. Series A: Mathematical and Physical Sciences*, vol. 434, no. 1890, pp. 9–13, 1991.